

Generation of pure single photon wavepackets by conditional preparation based on spontaneous parametric downconversion

Alfred B. U'Ren^{1,2}, Christine Silberhorn¹, Reinhard Erdmann³, Konrad Banaszek¹,

Warren P. Grice⁴, Ian A. Walmsley¹ and Michael G. Raymer⁵

¹ Clarendon Laboratory, Oxford University, Oxford, OX1 3PU, UK

² División de Física Aplicada, Centro de Investigación Científica y Educación Superior de Ensenada (CICESE), Baja California, 22860, Mexico

³ Rome Air Force Laboratory, Rome, NY, USA

⁴ Center for Engineering Science Advanced Research, Computer Science and Mathematics Division, Oak Ridge National Laboratory, Oak Ridge, Tennessee 37831, USA

⁵ Department of Physics and Oregon Center for Optics, University of Oregon, Oregon 97403, USA

(Dated: February 1, 2008)

We study the conditional-preparation of single photons based on parametric downconversion, where the detection of one photon from a given pair heralds the existence of a single photon in the conjugate mode. We derive conditions on the modal characteristics of the photon pairs which ensure that the conditionally prepared single photons are quantum mechanically pure. We propose specific experimental techniques which yield photon pairs ideally suited for single photon conditional preparation.

PACS numbers: 42.50.Ar, 03.67.-a

I. INTRODUCTION

Pure single photon states are probably the most fundamental entities in quantum optics, and constitute the starting point for many optically-based quantum enhanced technologies. A basic requirement for many key applications is the ability to generate reliably pure single photon wavepackets capable of high-visibility interference. Single photon wavepackets may be generated from number-correlated pairs by conditional state preparation. For example, photon pairs produced by the process of spontaneous parametric downconversion (PDC) in a $\chi^{(2)}$ non-linear medium allow conditional preparation of single photons, since the detection of one photon in the pair heralds the presence of the conjugate photon. PDC-generated photons have been employed for both fundamental tests of quantum mechanics and to demonstrate various quantum communication applications, such as quantum teleportation[1], quantum dense coding[2] and quantum cryptography[3].

A recent proposal for linear optical quantum computation (LOQC)[4] exploits the photon bunching that occurs in quantum interference between pure state single photons in conjunction with conditional state preparation in linear optical networks. There the detection of auxiliary photons indicates the successful operation of a given gate. For LOQC, as for all other applications involving optical quantum networks, high-visibility interference between photons from multiple sources is crucial. This necessitates, on the one hand, precise timing of the photons. This, in turn, demands a high probability of simultaneous generation from synchronized distinct sources. On the other hand, precise control of the modal structure of the generated photon pairs is essential to guarantee the purity of the conditionally prepared photon states. For PDC based implementations these re-

quirements lead to the need for a pulsed pump and for efficient sources exhibiting high brightness and detection efficiencies. Spatial modal control of the emitted photons, and a much increased production rate of photon pairs may result from waveguided PDC[5].

A common approach to guarantee indistinguishability in optical experiments uses strong spatial and spectral filtering. The cost of this, however, is a prohibitive reduction of the generation rate of usable single photon wavepackets. Since common birefringent phase-matching leads to spatial-spectral correlations with overlapping contributions, spatial filtering also causes optical losses for the signal photon for finite spectral filter bandwidths. As a consequence the fidelity of the conditionally prepared signal photons is limited due vacuum contributions. To eliminate these and to ensure, for example, successful gate operations in LOQC post-selecting by coincidence measurements is inevitable. But such post-selection, in turn, hinders the realization of scalable networks involving more than one or possibly two sources. Waveguided PDC is one route to accomplish both, to decorrelate the spatial degree of freedoms from spectral ones and to eliminate at the same time the spatial correlations between the PDC photons. This implies no need for spatial filtering, however, conditionally prepared single photons are in general still described by a mixed state due to spectral correlations present in the photon pairs. In this paper we study the conditional state preparation of single photon wavepackets based on PDC pumped by ultrafast pulses. We use a multi-mode description and propose novel engineering techniques for eliminating correlations between unobserved variables. This ensures that the detection of one photon from a given pair directly yields a pure single photon state in the conjugate mode, without resorting to filtering. The latter constitutes an important step for the further development of

quantum networks since it is expected to lead to an increase in the probability of simultaneous generation from multiple crystals by several orders of magnitude.

II. CONDITIONAL STATE PREPARATION OF PURE SINGLE PHOTON STATES IN A MULTIMODE DESCRIPTION

Single photon states are defined as containing a single quantum in the photon number basis. A complete specification of the photons requires that all degrees of freedom associated with the quantized electromagnetic field of the occupied optical modes must be taken into account. Thus, the complete description of the photons involves their polarization μ , their spatial vector \mathbf{r} or the wavevector \mathbf{k} , and their frequency ω or time dependence t . The dispersion relationship between \mathbf{k} and ω reduces one degree of freedom, such that we can restrict our analysis to transverse wavevectors \mathbf{k}^\perp . For simplicity we also consider only one single polarization, which is appropriate for PDC experiments aimed at conditional preparation of single photons. A pure single photon wavepacket then corresponds to a coherent superposition of monochromatic plane waves:

$$|\phi\rangle = N \int d\omega \int d\mathbf{k} c(\omega, \mathbf{k}) \exp[i(\mathbf{k} \cdot \mathbf{r} - \omega t)] \hat{a}^\dagger(\omega, \mathbf{k}) |0\rangle, \quad (1)$$

where N denotes the normalization constant and the coefficient function $c(\omega, \mathbf{k})$ determines the modal structure of the photon. The corresponding density operator is given by $\rho = |\phi\rangle\langle\phi|$ and exhibits nonzero off diagonal elements. This is to be contrasted with a completely mixed single photon state in frequency and momentum for which no coherence between the different modes exists and is characterized by a density operator of the form

$$\hat{\rho} = N \int d\omega \int d\mathbf{k} |c(\omega, \mathbf{k})|^2 \hat{a}^\dagger(\omega, \mathbf{k}) |0\rangle\langle 0| \hat{a}(\omega, \mathbf{k}), \quad (2)$$

which does not exhibit any off-diagonal elements.

In the process of PDC individual pump photons split into two daughter photons in modes \hat{a} and \hat{b} . For the purpose of conditional state preparation the modes \hat{a} and \hat{b} should be distinguishable in at least one degree of freedom, which might be polarization for type II phase-matching or the spatial degree of freedom for non-collinear phasematching. The interaction Hamiltonian of the $\chi^{(2)}$ -process for a strong pump field, which is treated classically, results in state of the approximate form:

$$|\Psi\rangle = |0\rangle|0\rangle + \mu \iint d\omega_s d\omega_i \iint d\mathbf{k}_s^\perp d\mathbf{k}_i^\perp \times F(\omega_s, \mathbf{k}_s^\perp; \omega_i, \mathbf{k}_i^\perp) \hat{\mathbf{a}}^\dagger(\omega_s, \mathbf{k}_s^\perp) \hat{\mathbf{b}}^\dagger(\omega_i, \mathbf{k}_i^\perp) |0\rangle \quad (3)$$

where μ is a measure of the efficiency of the PDC process and the function $F(\omega_s, \mathbf{k}_s^\perp; \omega_i, \mathbf{k}_i^\perp)$ represents a weighting function for the different spatial and spectral modes present, which results from the pump envelope and phasematching functions defined by the specific downconversion configuration[8]. It is assumed that

states of higher photon numbers can be ignored. The function $F(\omega_s, \mathbf{k}_s^\perp; \omega_i, \mathbf{k}_i^\perp)$ may contain correlations between the signal and idler photons in the spatio-temporal continuous degrees of freedom, thus yielding an entangled two-photon pair. A useful tool for analyzing such entanglement is that of carrying out a Schmidt decomposition [9] of the spatio-temporal state amplitude. The Schmidt decomposition entails expressing the two photon state in terms of complete basis sets of orthonormal states $A_n^\dagger|0\rangle$ and $B_n^\dagger|0\rangle$ such that:

$$|\Psi\rangle = \sum_n \sqrt{\lambda_n} \hat{A}_n^\dagger \hat{B}_n^\dagger |0\rangle \quad (4)$$

where $\sum_n \lambda_n = 1$ and where the values λ_n are known as the Schmidt coefficients. In this description the effective signal and idler creation operators \hat{A}_n^\dagger , \hat{B}_n^\dagger are given in terms of the Schmidt functions $\psi_n(\omega_s, \mathbf{k}_s^\perp)$ and $\phi_n(\omega_i, \mathbf{k}_i^\perp)$ as

$$\hat{A}_n^\dagger = \int d\mathbf{k}_s^\perp \int d\omega_s \psi_n(\omega_s, \mathbf{k}_s^\perp) \hat{a}^\dagger(\omega_s, \mathbf{k}_s^\perp) |0\rangle \quad (5)$$

and

$$\hat{B}_n^\dagger = \int d\mathbf{k}_i^\perp \int d\omega_i \phi_n(\omega_i, \mathbf{k}_i^\perp) \hat{b}^\dagger(\omega_i, \mathbf{k}_i^\perp) |0\rangle, \quad (6)$$

while the two-photon state amplitude $F(\mathbf{k}_s^\perp, \omega_s; \mathbf{k}_i^\perp, \omega_i)$ can be expressed as

$$F(\omega_s, \mathbf{k}_s^\perp; \omega_i, \mathbf{k}_i^\perp) = \sum_n \sqrt{\lambda_n} \psi_n(\omega_s, \mathbf{k}_s^\perp) \phi_n(\omega_i, \mathbf{k}_i^\perp), \quad (7)$$

where $\omega_{s,i}$ and $\mathbf{k}_{s,i}^\perp$ represent the wavelength and the transverse wavevector of the signal and idler photons. For the calculation of the Schmidt functions themselves the first step is to determine the reduced density matrices of the two sub-systems corresponding to the signal and idler photons, which are defined by

$$\hat{\rho}_s(\omega_s, \mathbf{k}_s^\perp; \tilde{\omega}_s, \tilde{\mathbf{k}}_s^\perp) = \iint d\omega' d\mathbf{k}'^\perp F(\omega_s, \mathbf{k}_s^\perp, \omega', \mathbf{k}'^\perp) \times F^*(\tilde{\omega}_s, \tilde{\mathbf{k}}_s^\perp, \omega', \mathbf{k}'^\perp) \quad (8)$$

and

$$\rho_i(\omega_i, \mathbf{k}_i^\perp; \tilde{\omega}_i, \tilde{\mathbf{k}}_i^\perp) = \iint d\omega' d\mathbf{k}'^\perp F(\omega', \mathbf{k}'^\perp, \omega_i, \mathbf{k}_i^\perp) \times F^*(\omega', \tilde{\mathbf{k}}_i^\perp, \tilde{\omega}_i, \mathbf{k}_i^\perp) \quad (9)$$

and as a second step solve the following the following integral eigen-value equations[9]:

$$\iint d\omega' d\mathbf{k}'^\perp \rho_s(\omega_s, \mathbf{k}_s^\perp, \omega', \mathbf{k}'^\perp) \psi_n(\omega', \mathbf{k}'^\perp) = \lambda_n \psi_n(\omega_s, \mathbf{k}_s^\perp) \quad (10)$$

$$\iint d\omega' d\mathbf{k}'^\perp \rho_i(\omega_i, \mathbf{k}_i^\perp, \omega', \mathbf{k}'^\perp) \phi_n(\omega', \mathbf{k}'^\perp) = \lambda_n \phi_n(\omega_i, \mathbf{k}_i^\perp) \quad (11)$$

thus yielding the Schmidt functions ψ_n and ϕ_n and the joint eigenvalues λ_n as Schmidt coefficients. The Schmidt decomposition simplifies the quantum state description, by turning the original state expressed as a quadruple integral over frequency and transverse momentum variables into a discrete sum, typically containing only a limited number of terms. The Schmidt functions $\psi_n(\omega_s, \mathbf{k}_s^\perp)$ and $\phi_n(\omega_i, \mathbf{k}_i^\perp)$ can be thought of as the basic building blocks of entanglement in the sense that if the signal photon is determined to be described by a function ψ_n , we know with certainty that its idler sibling is described by the corresponding function ϕ_n . The Schmidt modes also represent space-time localized wavepackets [6], and may be thought of as wavefunctions of a photon [7]. The probability of extracting a specific pair of modes $[\psi_n(\omega_s, \mathbf{k}_s^\perp), \phi_n(\omega_i, \mathbf{k}_i^\perp)]$ is given by the parameter λ_n , which is real and nonnegative. The amount of entanglement can be conveniently quantified by the cooperativity parameter [10] defined in terms of the Schmidt eigenvalues as:

$$K = \frac{1}{\sum_n \lambda_n^2}. \quad (12)$$

The value of K gives an indication of the number of active Schmidt mode pairs, which in turn is a measure of how much entanglement is present in the photon pairs. A two-photon state for which the cooperativity assumes its minimum allowed value $K = 1$ represents a state in which there is a single pair of active Schmidt mode functions and therefore exhibits no spectral or spatial entanglement. Another measure of the degree of non-separability is the so-called entropy of entanglement:

$$S = - \sum_n \lambda_n \log(\lambda_n) \quad (13)$$

which vanishes for a factorizable state, and increases monotonically with the amount of entanglement present.

For the conditional state preparation of single photon states via parametric down-conversion the idler photon is treated as a trigger, such that in the ideal case of perfect photon number correlations, a detection event of the trigger idler channel heralds the emission of a photon in the signal channel. The quantum state resulting from this conditional preparation can be obtained by modelling the trigger detection process in terms of a projection operator and tracing over the trigger channel photon:

$$\hat{\rho}_s = \text{Tr}_i(\hat{\rho}\hat{\Pi}). \quad (14)$$

Here the subscript i denotes a partial trace acting over the trigger idler mode, $\hat{\rho}$ is the density operator describing the two-photon PDC state, while $\hat{\Pi}$ is the measurement operator modelling the trigger photon detection. From the Schmidt decomposition it can be seen easily that filtering one specific Schmidt mode $\phi_n(\omega_i, \mathbf{k}_i^\perp)$ with the projection operator $\hat{B}_n^\dagger|0\rangle\langle 0|\hat{B}_n$ allows conditional preparation of a pure photonic wavepacket in the

signal mode. However this procedure requires coherent frequency-time and spatial filters, which are non-trivial to implement.

We thus proceed to investigate the synthesis of pure signal photons by time integrated detection of the trigger idler photon in combination with passive spectral and spatial pinhole filters. Correlations between the signal and idler photons generally lead to incoherence between different frequency and spatial components upon detection, which gives a mixed output signal state. The physical reason for this is that a measurement of the trigger reveals some information about the properties of the idler and hence destroys indistinguishability. A spatial and time-integrated detection of the idler state with a spectral interference filter with a profile function $\sigma(\omega)$ and a spatial filter of $\xi(k)$ can be modelled by the projection operator

$$\begin{aligned} \hat{\Pi} &= \int dt \int d\mathbf{r} \iint d\omega d\tilde{\omega} \iint d\mathbf{k} d\tilde{\mathbf{k}}^\perp \sigma(\omega) \xi(\mathbf{k}^\perp) \\ &\quad \times \exp[i(\mathbf{k} \cdot \mathbf{r} - \omega t)] \hat{b}^\dagger(\omega, \mathbf{k}) |0\rangle_i \langle 0| \hat{b}(\tilde{\omega}, \tilde{\mathbf{k}}) \\ &\quad \times \exp[-i(\tilde{\mathbf{k}} \cdot \tilde{\mathbf{r}} - \tilde{\omega} t)] \sigma^*(\tilde{\omega}) \xi^*(\tilde{\mathbf{k}}^\perp) \\ &= \int d\omega \int d\mathbf{k}^\perp |\sigma(\omega)|^2 |\xi(\mathbf{k}^\perp)|^2 \hat{b}^\dagger(\omega, \mathbf{k}) |0\rangle_i \langle 0|_i \\ &\quad \times \hat{b}(\omega, \mathbf{k}). \end{aligned} \quad (15)$$

By carrying out the calculation expressed by Eq. 14 using the density operator $|\Psi\rangle\langle\Psi|$ of the PDC state, it can be shown that the quantum state describing the signal channel, upon registering a trigger detection event, is given by

$$\begin{aligned} \hat{\rho}_s &= \int d\omega \int d\mathbf{k}^\perp \int d\omega_s \int d\mathbf{k}_s^\perp \int d\tilde{\omega}_s \int d\tilde{\mathbf{k}}_s^\perp \\ &\quad \times |\sigma(\omega)|^2 |\xi(\mathbf{k}^\perp)|^2 F(\omega_s, \mathbf{k}_s^\perp; \omega, \mathbf{k}^\perp) \hat{a}^\dagger(\omega_s, \mathbf{k}_s^\perp) \\ &\quad \times |0\rangle_s \langle 0|_s \hat{a}(\tilde{\omega}_s, \tilde{\mathbf{k}}_s^\perp) F^*(\tilde{\omega}_s, \tilde{\mathbf{k}}_s^\perp; \omega, \mathbf{k}^\perp). \end{aligned} \quad (16)$$

If we utilize the Schmidt decomposition of Eq. 7, the density operator of the conditionally prepared signal photon can be equivalently rewritten as

$$\begin{aligned} \hat{\rho}_s &= \sum_n \sum_m \sqrt{\lambda_n \lambda_m} \int d\omega \int d\mathbf{k}^\perp |\sigma(\omega)|^2 |\xi(\mathbf{k}^\perp)|^2 \\ &\quad \times \phi_n(\omega, \mathbf{k}^\perp) \phi_m^*(\omega, \mathbf{k}^\perp) \hat{A}_n^\dagger |0\rangle_s \langle 0|_s \hat{A}_m \end{aligned} \quad (17)$$

Under what conditions does $\hat{\rho}_s$ represent a pure state? Purity requires that the density operator ρ_s contain a single term, such that the signal state can be expressed in terms of a single Schmidt mode pair. From the expressions in Eq. 16 and Eq. 17 two approaches to achieve purity for the conditional state preparation via PDC become apparent. Restricting the trigger detection bandwidth to ideally one single spectral component, i.e. $|\sigma(\omega)| \rightarrow \delta(\omega - \Omega)$, as well as applying strong spatial filtering with an imaging lenses and a narrow pinhole, i. e. $|\xi(\mathbf{k}^\perp)| \rightarrow \delta(\mathbf{k}^\perp - \mathbf{K})$ effectively suppresses the integration over ω and \mathbf{k}^\perp in Eq. 16 and eliminates

the incoherent sum over different frequency and spatial components, leaving the signal photon in a monochromatic plane wave. Note, however, that this method for purification of the prepared signal output state necessarily implies diminishing count rates and approaches truly pure states only in the limit of vanishing counts. The Schmidt decompositions suggests an alternative route for the preparation of pure signal photon states exploiting PDC pair generation. If there exists only one Schmidt pair present, the sums in Eq. 17 disappear and the double integral term becomes an overall multiplicative constant. The latter implies that the prepared photon now forms a truly quantum-mechanically pure state. For a better understanding of this result we can relate the Schmidt decomposition to the correlations between the generated photons. The existence of only one Schmidt mode is actually equivalent to the statement that the PDC two-photon state is factorizable. Under such circumstances, the spectral and spatial properties of signal and idler photon are independent from each other so that the detection of the idler photon yields no information whatsoever about the signal photon. In order to further quantify the purity of the conditionally prepared single photons in the signal arm we can introduce the purity parameter p defined as

$$p = \text{Tr}(\hat{\rho}_s^2). \quad (18)$$

Evaluating the purity p in terms of the Schmidt decomposition, we can clarify the connection between purity of conditionally prepared *single photons* and the entanglement present in PDC *photon pairs*. In the absence of filters $p = \sum_n \lambda_n^2$, which is equivalent to $p = \frac{1}{K}$, where the cooperativity parameter K quantifies the entanglement of PDC. Thus, entanglement between the signal and idler photon hinders pure state preparation or, conversely, spatial and spectral separability (which can be enhanced by appropriate filters) ensures purity for conditional state preparation setups. This criteria delivers a valuable tool for engineering of PDC photon pair sources optimized for the generation of pure single photon states with without resorting to strong filtering and illustrates the necessity of decoupling the signal and idler photons in all degrees of freedom.

III. SPECTRALLY DECORRELATED TWO-PHOTON STATES

As shown in section II, the generation of pure single photon wavepackets based on PDC photon pairs necessitates that all correlations between the signal and idler photons be eliminated. This includes correlations in all degrees of freedom including spectral, transverse momentum and polarization. Since the full discussion of all degrees of freedom is beyond the scope of this paper, for the discussion following we assume that the spatial modes of the PDC photon pairs are independently rendered decorrelated. Such spatial decorrelation can be achieved, for

example, by waveguided PDC[5], in which the photons may be emitted only into specific transversely-confined modes. In addition, some of the techniques to be presented here designed to obtain spectral decorrelation for bulk crystals, could be extended to the spatial domain.

A number of techniques have been proposed to generate photon pairs exhibiting spectral decorrelation without resorting to spectral filtering. Grice *et al.* showed[11] that an avenue towards such states is the group velocity matching condition derived by Keller *et al.*[12]. Such a technique is extended here, showing that if an additional condition between the pump chirp and the crystal dispersion is fulfilled, factorizability of the joint spectral *amplitude* is guaranteed. Considering the complete joint amplitudes rather than restricting attention to intensity correlations is important, because correlations in the phase terms of the joint spectral amplitude, which are not apparent in the joint spectral intensity, can introduce correlations in the times of emission. Thus, in order to guarantee full signal-idler decorrelation, the joint spectral *amplitude* (and therefore the joint spectral intensity) must be factorizable.

It has likewise been shown that a spectrally decorrelated state may be obtained by exploiting transverse momentum in a bulk $\chi^{(2)}$ type-I crystal[14]. Specifically, this is achieved using of a focused Gaussian pump beam with a spot size fulfilling a certain relationship with the crystal length. Walton *et al.* have recently reported a different scheme in which a transverse pump generates counter-propagating spectrally de-correlated photon pairs[15]. The essential advantage of these two techniques is that spectral decorrelation may be obtained at any wavelength where phasematching is possible, as opposed to the technique based on group velocity matching which occurs for quite restrictive frequency regimes.

In this paper we also introduce a novel technique, based on a sequence of crystals with intermediate birefringent spacers. In this scheme—although group velocities are not matched to each other—the maximum group velocity mismatch observed can be limited to an arbitrarily small value. Furthermore, spectral decorrelation, as well as a more general class of spectrally engineered photon pairs, may be obtained at any wavelength where phasematching is possible[19].

A. Group velocity matching

The general expression for the joint probability amplitude of the two-photon state generated in the process of PDC in the ultrashort pulsed pump regime (and assuming fixed directions of propagation) is given by

$$f(\omega_s, \omega_i) = \alpha(\omega_s, \omega_i)\phi(\omega_s, \omega_i) \quad (19)$$

where the pump envelope function $\alpha(\omega_s, \omega_i)$, modelled here by a Gaussian in terms of the frequency detunings

from the central PDC frequency $\nu_\mu = \omega_\mu - \omega_0$:

$$\alpha(\nu_s + \nu_i) = \exp \left[- \left(\frac{\nu_s + \nu_i}{\sigma} \right)^2 \right] \quad (20)$$

and where the so-called phasematching function $\phi(\omega_s, \omega_i)$ describing the optical properties of the nonlinear crystal is expressed as[8]:

$$\phi(\omega_s, \omega_i) = \text{sinc} \left(\frac{L\Delta k(\omega_s, \omega_i)}{2} \right) e^{i\frac{L\Delta k}{2}} \quad (21)$$

in terms of the phase mismatch:

$$\Delta k(\omega_s, \omega_i) = k_s(\omega_s) - k_i(\omega_i) - k_p(\omega_p). \quad (22)$$

We will at this point restrict our attention to a frequency-degenerate process, i.e. the Taylor expansion for each of the two photons is assumed to be centered at the same frequency, ω_0 . We can then express the phase-mismatch Eq. 22 as a Taylor expansion up to second order:

$$L\Delta\tilde{k}(\nu_s, \nu_i) = L\Delta k^0 + \tau_s\nu_s + \tau_i\nu_i + \beta_s\nu_s^2 + \beta_i\nu_i^2 + \beta_p\nu_s\nu_i + O(\nu^3) \quad (23)$$

with

$$\Delta k^0 = k_s(\omega_0) + k_i(\omega_0) - k_p(2\omega_0) \quad (24)$$

representing the constant term of the Taylor expansion, which must vanish to guarantee phase-matching; $O(\nu^3)$ denotes terms of third and higher order and $(\mu = s, i)$

$$\begin{aligned} \tau_\mu &= L [k'_\mu(\omega_0) - k'_p(2\omega_0)] = L (u_\mu^{-1} - u_p^{-1}) \\ \beta_\mu &= \frac{L}{2} [k''_\mu(\omega_0) - k''_p(2\omega_0)] \\ \beta_p &= Lk''_p(2\omega_0). \end{aligned} \quad (25)$$

In the previous expressions ' and '' denote first and second derivatives with respect to frequency (evaluated at ω_0 in the case of the signal and idler wave vectors and at $2\omega_0$ in the case of the pump wavevector). u_p represents the pump group velocity whereas u_μ ($\mu = s, i$) represents the group velocity experienced by each of the signal and idler photons.

We will use the additional approximation of expressing the sinc function in the phasematching function as a Gaussian function through the approximation:

$$\text{sinc}(x) \approx e^{-\gamma x^2} \text{ with } \gamma = .193\dots \quad (26)$$

where the numerical value of γ results from the condition that both functions exhibit the same FWHM. We will further allow the pump field to carry a quadratic phase to account for chirp. Under such circumstances, the joint

spectral amplitude is given as:

$$\begin{aligned} \tilde{f}(\nu_s, \nu_i) &= \\ M &\exp \left[- \left(\frac{\nu_s + \nu_i}{\sigma} \right)^2 \right] \exp [i\beta_t(\nu_s + \nu_i)^2] \\ &\times \exp \left[- \frac{\gamma}{4} (\tau_s\nu_s + \tau_i\nu_i)^2 \right] \\ &\times \exp \left[i\frac{1}{2} (\tau_s\nu_s + \tau_i\nu_i + \beta_s\nu_s^2 + \beta_i\nu_i^2 + \beta_p\nu_s\nu_i) \right] \end{aligned} \quad (27)$$

where M is a normalization constant and β_t is the GVD dispersion term which the pump experiences prior to the crystal. We note that the above expression contains, within the regime of the approximations used all terms up to quadratic order in the frequency detunings. By expanding the exponential terms we can express the joint spectral amplitude as

$$\begin{aligned} \tilde{f}(\nu_s, \nu_i) &\propto \\ &\exp \left[- \left(\frac{1}{\sigma^2} + \frac{\gamma}{4}\tau_s^2 \right) \nu_s^2 \right] \exp \left[i\frac{\tau_s}{2}\nu_s + i \left(\beta_t + \frac{\beta_s}{2}\nu_s^2 \right) \right] \\ &\times \exp \left[- \left(\frac{1}{\sigma^2} + \frac{\gamma}{4}\tau_i^2 \right) \nu_i^2 \right] \exp \left[i\frac{\tau_i}{2}\nu_i + i \left(\beta_t + \frac{\beta_i}{2}\nu_i^2 \right) \right] \\ &\times \exp \left[-2 \left(\frac{1}{\sigma^2} + \frac{\gamma}{4}\tau_s\tau_i \right) \nu_s\nu_i + i \left(2\beta_t + \frac{\beta_p}{2} \right) \nu_s\nu_i \right]. \end{aligned} \quad (28)$$

Here the contributions depending on ν_s and ν_i exclusively and those depending on both ν_s and ν_i are written as separate factors, and phase terms linear in ν_μ have been dropped. We can see from Eq. 28 that any unfactorizability resides in the mixed term containing an argument proportional to $\nu_s\nu_i$. Furthermore, we can now easily see that the conditions that guarantee a factorizable state (i.e. that make the mixed term vanish) are:

$$\frac{4}{\sigma^2} + \gamma\tau_s\tau_i = 0 \quad (29)$$

and

$$2\beta_t + \frac{\beta_p}{2} = 0. \quad (30)$$

We note that the second condition [Eq. 30] refers to phase contributions in the joint spectral amplitude, and was not included in the earlier work by Grice *et al.*[11]. Because such phase contributions play no role in the intensity, the fulfilment of the first of the derived conditions [Eq. 29] is sufficient to obtain a factorizable joint spectral *intensity*. If both conditions [Eqns. 29 and 30] are satisfied, the two-photon state is guaranteed to be free of correlations in the spectral and temporal domains, as indicated by a factorizable joint spectral *amplitude*. We now analyze the effects of the first condition on the two photon state. If condition Eq. 29 is fulfilled, we may express the joint spectral intensity as:

$$S(\omega_s, \omega_i) = |f(\omega_s, \omega_i)|^2 \propto \exp \left[-2\frac{\nu_s^2}{\sigma_s^2} \right] \exp \left[-2\frac{\nu_i^2}{\sigma_i^2} \right] \quad (31)$$

where the spectral widths σ_s and σ_i are given by:

$$\sigma_\mu = \frac{2\sigma}{\sqrt{4 + \gamma\sigma^2\tau_\mu^2}} \quad (32)$$

with $\mu = s, i$. Thus we have confirmed that such a joint spectral intensity exhibits the desired factorizability. The ratio of the larger of the two spectral widths (for signal and idler) to the smaller one, to be referred to as the aspect ratio, (i.e. a measure of the degree of elongation exhibited by the two-photon spectral distribution in $\{\omega_s, \omega_i\}$) is given by:

$$r = \max \left\{ \frac{\sigma_s}{\sigma_i}, \frac{\sigma_i}{\sigma_s} \right\} = \sqrt{\frac{4 + \gamma\sigma^2\tau_1^2}{4 + \gamma\sigma^2\tau_2^2}}. \quad (33)$$

where $\tau_1 = \tau_s$ and $\tau_2 = \tau_i$ if $\sigma_s > \sigma_i$ and likewise $\tau_1 = \tau_i$ and $\tau_2 = \tau_s$ if $\sigma_i > \sigma_s$. In what follows the aspect ratio will prove to be a useful tool in the characterization of the two-photon state.

Let us now consider the effect of the second of the derived conditions [Eq. 30]. We will start by analyzing the effect of the phase terms present in the joint spectral amplitude [Eq. 28] on the photon pair correlations. First, the linear phases $i\tau_\mu\nu_\mu$ (with $\mu = s, i$) shift the times of emission with respect to the pump pulse for each of the two single photon wavepackets. The fact that for a type-II interaction $\tau_s \neq \tau_i$ implies that the two single-photon wavepackets forming a given photon pair are emitted at different mean times, where the mean emission time difference is simply $\tau_s - \tau_i$. This temporal walkoff can be compensated by means of a relative delay between the signal and idler photons introduced after the crystal. While the GVD terms (β_s, β_i and β_p) have no effect on the joint spectral *intensity* of the two-photon state (in the regime of the approximations used which neglects contributions of cubic and higher order terms in the frequency detunings) they translate into broadening in the temporal domain, which becomes apparent upon a Fourier transformation of the joint spectral amplitude to obtain the joint temporal amplitude. The quadratic phase $i(\beta_t + \beta_\mu/2)\nu_\mu^2$ (with $\mu = s, i$) results in uncorrelated temporal broadening of the two photon wavepackets along the t_s and t_i axes. The temporal broadening is proportional to the crystal length and is, in general, different for each of the two photons[20] (since $\beta_s \neq \beta_i$). The mixed term, proportional to $\nu_s\nu_i$, introduces correlations in the times of emission. This means that decorrelations of spectral intensity are not sufficient for true single mode photon pair generation. We note that it is the β_p term which is responsible for extirpating the factorizability. Therefore, if it were possible to eliminate the effect of β_p , the two-photon joint temporal amplitude would broaden in such a way that the decorrelated character is maintained. Fortunately, it is possible to compensate for the presence of β_p simply by letting the incoming pump field have a chirp (quadratic phase) which fulfils our second derived factorizability condition (Eq. 30). The quadratic

phase which the pump should carry is therefore given by: $\beta_t = -\beta_p/4$. We also note that it is in principle possible to ‘‘tune’’ the degree of temporal correlation in the two-photon state (and therefore the level of distinguishability in an interference experiment) by using a pump field with a variable chirp, *i. e.* variable β_t .

Let us return to the first of the conditions derived for factorizability [Eq. 29]. This condition may be written in terms of the crystal and pump field parameters as:

$$\frac{4}{\sigma^2} + \gamma L^2(k'_s - k'_p)(k'_i - k'_p) = 0 \quad (34)$$

where σ is the pump bandwidth, L is the crystal length, k'_p represents the first frequency derivative of k_p evaluated at $2\omega_0$, k'_μ ($\mu = s, i$) represents the first frequency derivative of k_μ evaluated at ω_0 and $\gamma \approx .193$. For specific experimental situations, pairs of values for the pump bandwidth σ and the crystal length L may exist such that the above condition (Eq. 34) is fulfilled. Note that for the condition in Eq. 34 to be fulfilled, one of the following must be true: $k'_s < k'_p < k'_i$ or $k'_i < k'_p < k'_s$, *i. e.* the group velocity of the pump must lie between that of the signal and idler. None of the experiments recently reported in the literature make use of crystals meeting the above requirements. This should not be surprising, since it requires a material in which one of the daughter photons has a smaller group velocity than the pump, which necessarily has a shorter wavelength. Alternatively, this condition may be expressed as the requirement that τ_s and τ_i have opposite signs.

In order to get further physical insight, consider the phasematching condition resulting from the approximation of neglecting second and higher order terms in the Taylor expansion (and assuming that the constant term vanishes). In this case the phasematching condition [see Eq. 22] becomes:

$$\tau_s\nu_s + \tau_i\nu_i = 0 \quad (35)$$

The contour in $\{\nu_s - \nu_i\}$ space defined by perfect phase-matching is therefore a straight line with slope $-\tau_s/\tau_i$. In other words the angle subtended by the ν_s axis and the perfect phasematching contour is given by:

$$\theta_{II} = -\arctan\left(\frac{\tau_s}{\tau_i}\right) = -\arctan\left(\frac{k'_s - k'_p}{k'_i - k'_p}\right) \quad (36)$$

where the II subscript refers to type-II phasematching. Note that the angle θ_{II} does not depend on the crystal length; it is solely a property of the dispersion of the material at the particular PDC wavelength. For type-I PDC, $\tau_s = \tau_i$ so that a similarly defined angle has the fixed value $\theta_I = -45^\circ$. Thus, the condition that $k'_s - k'_p$ and $k'_i - k'_p$ have opposite signs cannot be met with type-I PDC while in the case of type-II it translates into the requirement that the slope of the perfect phasematching contour be positive.

Let us now consider a specific case fulfilling the positive slope requirement: the case where the slope of the perfect

phasematching contour is unity, i.e. $\theta_{PM} = 45^\circ$. It is straightforward to show from Eq. 36 that the condition which guarantees such a unit slope is given by:

$$\frac{k'_s + k'_i}{2} = k'_p \quad (37)$$

which says that the average inverse group velocities for the signal and idler photons equals the pump inverse group velocity. This condition, which can be alternatively expressed as $\tau_s + \tau_i = 0$, is referred to as the group velocity matching condition [11, 12]. We can picture this condition as the requirement that the signal and idler photons are temporally delayed with respect to the pump in a symmetric way, with the two PDC photons delayed in opposite directions, by the same amount, from the pump. Alternatively we may interpret the group velocity matching condition Eq. 37 for a factorizable two-photon state in terms of the joint spectral intensities and identify that the aspect ratio [see Eq. 33] evaluates to unity. The latter implies that the factorizable joint spectral intensity exhibits a circular shape on the $\nu_s - \nu_i$ plane. Such symmetry is crucial for experiments which rely on classical interference between signal and idler PDC modes, since it can then fulfil the requirement of ideal signal-idler spectral mode matching and lead to unit visibility in the conventional Hong-Ou-Mandel experiment[13]. Hence in this configuration the generated PDC two photon state exhibits signal-idler mode matching as well as the factorizability required for ideal conditional preparation of pure single photons, and therefore constitutes a versatile two-photon state, useful for a broad class of experiments[14].

B. Asymmetric group velocity matching

In the context exclusively of generating single pure single photon states, each of the crystals used must generate factorizable (but not necessarily symmetric) two-photon states in order to guarantee unit interference visibility in a multi-crystal experiment where only signal or respectively idler photons are superimposed on each other. Thus, in this context, a non-unit aspect ratio is indeed not a limitation (as long as the elongation is “aligned” with the frequency and time axes). In this section we study experimental situations where it is in fact desirable to obtain a state exhibiting a spectrally “elongated” shape and thus a high aspect ratio.

The first condition for frequency decorrelation (Eq. 29) can in fact be met for several common $\chi^{(2)}$ crystals. For example, in the case of periodically-poled KTP (PP-KTP) (in degenerate collinear operation), it can be met for configurations where the PDC central wavelength is within the range $1.207\mu\text{m} < \lambda < 2.364\mu\text{m}$ (see also Ref. [16]). Within this range only the particular wavelength of $\lambda = 1.568\mu\text{m}$ fulfills the group velocity matching condition (Eq. 37), which yields the unit-aspect ratio two-photon state, while the aspect ratio departs from unity for all other wavelengths. The lower and upper

bounds correspond to two-photon states characterized by a high aspect ratio with asymmetric joint spectral intensities, though maintaining “alignment” with the ν_s and ν_i axes). In Ref. [11], it was similarly established that in the case of BBO factorizability may be obtained for wavelengths between 1.169nm and 1.949nm with the group velocity matching condition fulfilled at 1.514nm. This spectral regio is of great importance for optical quantum communication using optical fibers. Unfortunately for the materials discussed above, frequency-decorrelated PDC (and specifically unit aspect ratio decorrelated states) occurs at wavelengths at which single-photon detectors are not well-developed. Although InGaAs avalanche photodiodes have been shown to be capable of photon counting at such longer wavelengths[17], quantum efficiencies are rather low (about 15%) while dark count control necessitates cryostatic cooling. Thus, frequency decorrelated two-photon states, which occur for available crystal materials at longer $> 1\mu\text{m}$ wavelengths, present acute experimental challenges mainly in terms of detection. In what follows we will discuss the synthesis of factorizable two-photon states in arbitrary spectral region, with a view to accessing an experimentally more convenient range.

We begin our analysis by re-writing the condition for factorizability (see Eq. 34) as:

$$\frac{4}{\sigma\tau_s} + \gamma\sigma\tau_i = 0. \quad (38)$$

Consider this condition in the long PDC crystal regime. Recall that the temporal walkoff terms τ_s and τ_i are each proportional to the crystal length L . Thus, we see that if $\tau_s \gg \sigma^{-1}$ (as is the case in the limit $L \rightarrow \infty$), the condition reduces to the simpler constraint: $\tau_i = 0$: i.e. the latter tells us that spectral decorrelation can be achieved employing a long crystal while making one of the temporal walkoff terms vanish. Because in this variant of the technique the pump group velocity is matched to that of one of the PDC photons (but not to both) we refer to this technique as asymmetric group-velocity matching. Note that for a given crystal length L the frequency decorrelation condition [Eq. 34] can in general be met at most for one particular value of the pump bandwidth σ ; i.e. there is a strict one to one relationship between crystal length L and the pump bandwidth σ required for spectral factorizability. The latter can be an experimental limitation if for example the pump bandwidth cannot be easily modified. In the long crystal regime, however, the condition becomes independent of the pump bandwidth σ . The fact that a frequency decorrelated two-photon state may thus be synthesized irrespective of the pump bandwidth makes such a long crystal PDC a more flexible source of spectrally-engineered photon pairs. In such a long-crystal source, varying the pump bandwidth merely alters the aspect ratio without affecting the spectral decorrelation.

Fortunately it is possible to obtain a decorrelated two-photon state (albeit with a high aspect ratio) at wavelengths suitable for room-temperature operated silicon-

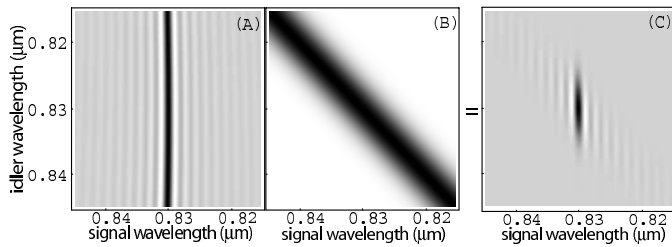


FIG. 1: High aspect ratio decorrelated two-photon state obtained by degenerate collinear PDC from a 2cm-long KDP crystal exhibiting a cut angle of 67.77° . (A) “Vertical” phasematching function exhibiting asymmetric group velocity matching (B) Pump envelope function describing a pump pulse centered at 415nm with a spectral bandwidth of 5nm. (C) Resulting factorizable two-photon state.

based avalanche photodiodes. These detectors can exhibit both $\sim 60\%$ quantum efficiency as having a manageable level of dark counts. Figure 1 shows a two-photon state produced by collinear degenerate type-II PDC in a 2cm-long KDP crystal cut at a phasematching angle of 68° yielding photon pairs centered at 830nm. Note that although the spectral distribution is elongated, factorizability is exhibited and hence pure conditional pure state generation (see Sec. II) is ensured. It is also interesting to notice that—in contrast to general PDC—such a state is predicted to yield conditionally prepared photon states which are Fourier transform limited[18]. The two-photon state features a narrow spectrum for the ordinary-ray photon and a broader one for the extraordinary-ray photon. This arises from the matching of the group velocity on the pump photons to that of the o-ray photon, but not to the e-ray photon.

In summary, our proposed long-crystal KDP-source yielding spectrally factorizable photon pairs, based on asymmetric group velocity matching, is characterized by the following properties: 1) If it is used for conditional single photon generation the prepared photons are described by quantum mechanically pure states. This property is evident in the by Fourier transform limited character of the photonic wavepackets. 2) Narrow spectral bandwidth ordinary-ray photons allow spectral filtering to eliminate any background light without discarding PDC photons. If the filtered mode is then used as a trigger in a conditional source of single photons, the resulting photon exhibits the largest spectral bandwidth allowed by the pump bandwidth. 3) The decorrelated character is independent of the pump bandwidth, thus eliminating an important experimental constraint[21]. 4) The generated state requires a pump centered at 415nm, easily accessible with a frequency-doubled Titanium sapphire laser, while the produced photons at 830nm can be efficiently detected with Silicon-based single photon counting modules. Even though KDP has a smaller non-linearity than other common $\chi^{(2)}$ materials such as BBO, the long crystal used translates into a gain in production rate of photon pairs with respect to typical PDC sources

based on shorter crystals. 5) KDP crystals at a $\sim 70^\circ$ cut angle exhibit a relatively small transverse walkoff; at a pump wavelength of 415nm the walkoff angle is 1.15° giving, for a 2cm long crystal a lateral displacement of just over $400\mu\text{m}$. We note, however, that used as a conditional source of single photons in networks where signal and idler modes are not superimposed, the walkoff exhibited is not a limitation, as the signal and idler photons need not be indistinguishable from each other. 6) As will be discussed in the next section, such a high aspect ratio factorizable state additionally exhibits an interesting dispersion insensitivity effect.

C. Dispersion insensitivity in long-crystal asymmetrically group velocity matched photon pairs

As was discussed above, broadening of the joint spectral amplitude results from GVD terms, which [see Eqns. 25] are proportional to the crystal length. Thus, increasing the crystal length used leads to a temporally-broader two-photon time of emission distribution. If the mixed term phase $2\beta_t + \frac{\beta_p}{2}$ in Eq. 28 does not vanish, such broadening eliminates the “alignment” with the time axes. However, in this section we will show that, for high-aspect ratio spectrally factorizable two-photon states, in the long-crystal regime the mixed term responsible for introducing correlations in the times of emission, can be made arbitrarily small (even temporal broadening still occurs). In fact, an increase in crystal length gives a net reduction of temporal correlations.

Let us assume that the crystal length and pump bandwidth are chosen so that the first condition for factorizability (Eq. 29) is satisfied. Under these circumstances (see Eq. 31), the joint spectral amplitude may be expressed as:

$$f(\omega_s, \omega_i) = \exp\left[-\frac{\nu_s^2}{\sigma_s^2}\right] \exp\left[-\frac{\nu_i^2}{(r\sigma_s)^2}\right] \times \exp\left[i(\beta_s\nu_s^2 + \beta_i\nu_i^2 + \beta_p\nu_s\nu_i)\right] \quad (39)$$

where we have expressed the idler width in terms of the aspect ratio r as $\sigma_i = r\sigma_s$ and where the GVD terms (β_s , β_i and β_p) were defined in Eq. 25. Note that because in the above expression the lack of factorizability resides in the phase term, the joint spectral *intensity* is factorizable. Nevertheless the presence of a mixed phase term, proportional to β_p , translates into lack of factorizability in the temporal domain. In order to study the temporal properties of the wavepacket, let us carry out a Fourier transform of the above joint spectral amplitude, to obtain the following joint temporal intensity:

$$\begin{aligned} \mathcal{S}(t_s, t_i) &= |\mathcal{F}(t_s, t_i)|^2 \\ &= \exp\left[-\frac{2t_s^2}{\delta t_s^2}\right] \exp\left[-\frac{2t_i^2}{\delta t_i^2}\right] \exp\left[-2\sigma_M^2 t_s t_i\right] \end{aligned} \quad (40)$$

where the temporal wavepacket width along t_s is given

in terms of the reciprocal aspect ratio $s = r^{-1}$ by:

$$\delta t_s = \frac{2\sqrt{2}\sqrt{2 + \sigma_s^4(2\beta_s^2 + \beta_p^2 s^2 + 2\beta_i^2 s^4)}}{\sigma_s\sqrt{4 + \sigma_s^4(\beta_p^2 + 4\beta_i^2 s^2)}}, \quad (41)$$

the temporal wavepacket width along t_i is given by:

$$\delta t_i = \frac{2\sqrt{2}\sqrt{2 + \sigma_s^4(2\beta_s^2 + \beta_p^2 s^2 + 2\beta_i^2 s^4)}}{s\sigma_s\sqrt{4 + \sigma_s^4(4\beta_s^2 + 4\beta_p^2 s^2)}}, \quad (42)$$

and

$$\sigma_M^2 = \frac{\sigma_s^6 s^2 \beta_p (\beta_s + \beta_i s^2)}{2(2 + \sigma_s^4(2\beta_s^2 + \beta_p^2 s^2 + 2\beta_i^2 s^4))} \quad (43)$$

represents the mixed term coefficient. Specializing to a high aspect ratio spectrally factorizable state such as one produced by the long KDP crystal source discussed in the last section, the temporal walkoff between pump and the ordinary-ray photon τ_o vanishes. Thus, according to Eq. 32 the ordinary-ray spectral width is then given by $\sigma_s = \sigma$ where σ represents the pump bandwidth. Likewise, in the long-crystal limit, according to Eq. 32 the idler spectral width is given by $1/(\sqrt{\gamma}\tau_e)$. This leads to the following expression for the reciprocal aspect ratio:

$$s = \frac{2}{\sqrt{\gamma}\sigma(k'_s - k'_p)L}. \quad (44)$$

Note, from the above expression, that the reciprocal aspect ratio s is inversely proportional to the crystal length L . This fact, together with the linear dependence of each of the GVD terms (β_s, β_i and β_p) on the crystal length L can be used to express the mixed term coefficient σ_M^2 in terms of its overall length dependence. We thus obtain:

$$\begin{aligned} \sigma_M^2 &\approx \frac{\sigma^6 s^2 \beta_p \beta_s}{4(1 + \sigma^4 \beta_s^2)} \\ &= \frac{\sigma^4 k'_p (k'_s - k'_p)}{4\gamma(k'_i - k'_p)^2 [1 + \sigma_p^4 L^2 (k'_s - k'_p)^2]}. \end{aligned} \quad (45)$$

The net crystal length dependence of σ_M^2 in the long-crystal regime is inverse quadratic. Hence increasing the crystal length does not lead to an increase in magnitude of the mixed term, but actually reduces the correlations. Recall that for a factorizable high aspect ratio two photon state, the pump bandwidth σ and crystal length L do not have to be specified jointly *i.e.* there is no relationship that should be fulfilled between them to ensure factorizability. Together with the dispersion insensitivity, the latter means that the crystal can be made arbitrarily long without introducing temporal correlations. The main remaining considerations using a long crystal are excessive temporal broadening and absorption of PDC photons in the crystal. We note that if the pump field is chirped, β_p should be substituted by $2\beta_t + \frac{\beta_p}{2}$ in the expressions

for the mixed term, Eqns. 43 and 45 (where β_t is introduced in Eq. 28 represents the quadratic phase carried by the pump field). The presence of chirp in the pump pulse can be treated similarly: upon increasing the crystal length L , the magnitude of the mixed term decreases. Thus, we conclude that (within the regime of validity of the approximations used) the source presented here is insensitive to those dispersive effects leading to the appearance of temporal correlations, either introduced in the PDC crystal itself or indeed prior to the crystal.

We can understand the dispersion insensitivity effect described above by realizing that dispersion effects in general require not only the presence of a dispersive phase but also broadband light. Engineering the joint spectral intensity by making it nearly monochromatic along either the signal or the idler axis, means that the resulting narrowband photon will experience limited dispersion. Furthermore, the mixed term (leading to temporal correlations) is also reduced by the monochromaticity of one of the photons. Fig. III C shows for the two-photon state produced by collinear degenerate type-II PDC in a 2cm-long KDP crystal cut at a phasematching angle of 68° yielding photon pairs centered at 830nm. The joint *spectral* intensity is shown in Fig. III C(A) while the joint *temporal* intensity in Fig. III C(B). Because the parameters of the source fulfil Eq. 34, the joint spectral intensity is factorizable. Furthermore, the joint temporal intensity is also factorizable, for arbitrarily long crystals. Thus, the two-photon state produced by such a two-photon source is free from spectral (temporal) correlations, making it an ideal source of conditionally prepared pure and Fourier-transform limited single photon wavepackets.

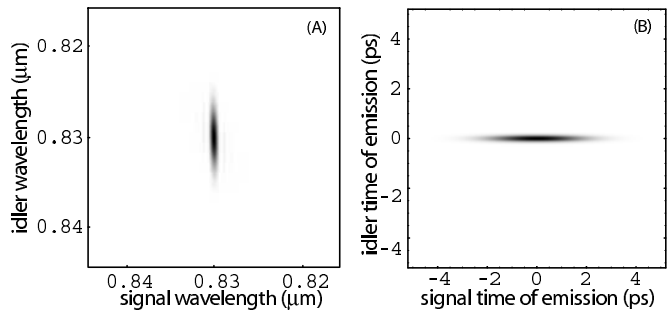


FIG. 2: High aspect ratio two-photon state obtained by degenerate collinear PDC from a 2cm-long KDP crystal exhibiting space time decorrelation (A) Factorable joint *spectral* intensity (B) Factorable joint *temporal* intensity.

IV. TWO PHOTON STATE ENGINEERING VIA CRYSTAL SEQUENCES WITH BI-REFRACTIVE COMPENSATORS

As has been shown in this paper, group velocity matching is a powerful technique which enables the engineering of two photon states with desirable properties, tai-

lored for specific applications. Nevertheless, group velocity matching crucially depends on the dispersion exhibited by the pump, signal and idler fields in the nonlinear crystal used, and tends to occur only in specific wavelength ranges. In this section we propose and analyse a technique in which the group velocity mismatch can be controlled at arbitrary wavelengths. This comes at the cost, however, of an increased source complexity. In this scheme, a *sequence* of nonlinear crystals is used interspersed with birefringent spacers exhibiting a dispersion such that the group velocity mismatch introduced by the crystal is compensated for by that in the spacer. This scheme can be thought of as analogous to band gap engineering using photonic crystals, except that group velocity, rather than phase velocity, is compensated.

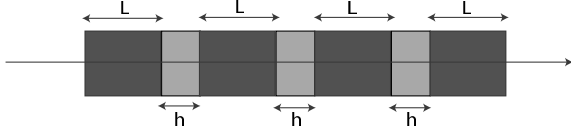


FIG. 3: This figure shows a schematic of the proposed crystal sequence with intermediate bi-refracting spacers. Each crystal has a length L while each spacer has a length h .

Consider the experimental arrangement shown in Fig. 3 consisting of N identical $\chi^{(2)}$ crystals and $N - 1$ linear $\xi^{(1)}$ spacers. Each of the crystals is assumed to be cut and oriented for degenerate collinear type-II PDC while the compensators are assumed not to exhibit a $\chi^{(2)}$ nonlinearity. It is further assumed that each crystal has length L while each spacer has length h . The phase mismatch in each of the crystals is given by

$$\Delta k = k_p - k_s - k_i \quad (46)$$

where k_μ (with $\mu = p, s, i$) denotes the wavenumber for each of the three fields taking into account dispersion in the crystal. The phase mismatch introduced by each of the spacers is equivalently given by:

$$\Delta \kappa = \kappa_p - \kappa_s - \kappa_i. \quad (47)$$

where κ_μ (with $\mu = p, s, i$) now represents the wavenumber for each of the three fields taking into account dispersion in the birefringent spacer. For an assembly of N crystals and $N - 1$ spacers the overall phasematching function can then be calculated as

$$\begin{aligned} \phi_N(\Delta k, \Delta \kappa) &= \sum_{m=0}^{N-1} e^{im(L\Delta k + h\Delta \kappa)} \text{sinc} \left[\frac{L}{2} \Delta k \right] \\ &= e^{\frac{i(N-1)\Phi}{2}} \frac{\sin(\frac{N\Phi}{2})}{\sin(\frac{\Phi}{2})} \text{sinc} \left[\frac{L\Delta k}{2} \right] \end{aligned} \quad (48)$$

where we defined the quantity Φ as

$$\Phi = L\Delta k + h\Delta \kappa. \quad (49)$$

Hence, apart from an overall phase factor the crystal assembly phasematching function is composed of the product of two distinct functions: one corresponds to the

phasematching function of a single crystal and the second factor incorporates the combined effect of the crystal and spacer dispersion. In order to carry out more explicit calculations, it is helpful to write down the crystal and spacer phasemismatch as a Taylor expansion [similar to that in Eq. 23, however here we omit all terms of orders higher than $O(\nu^2)$]. Thus, we obtain, in terms of the frequency detunings $\nu_\mu = \omega_\mu - \omega_0$ (with $\mu = s, i$):

$$\Phi = L\Delta k^{(0)} + h\Delta \kappa^{(0)} + T_s \nu_s + T_i \nu_i \quad (50)$$

where $L\Delta k^{(0)}$ and $h\Delta \kappa^{(0)}$ denote the constant terms of the Taylor expansions for the crystal and spacer phase mismatch terms and

$$T_\mu = [k'_p(2\omega_0) - k'_\mu(\omega_0)] L + [\kappa'_p(2\omega_0) - \kappa'_\mu(\omega_0)] h \quad (51)$$

with $\mu = s, i$ constitutes the first-order coefficients of the expansion. The term $\Delta k^{(0)}$ vanishes under the assumption that each of the crystals is aligned such that phasematching is attained.

We can now analyze the influence of the proposed crystal and birefringent compensator assembly on the joint spectral correlations and introduce a new function

$$\Upsilon_N(x) = \frac{1}{N} \frac{\sin(Nx)}{\sin(x)}, \quad (52)$$

which describes the modifications to the spectral structure of the phasematching function [see Eq. 48]. As depicted in Fig. IV the function $\Upsilon_N(x)$ exhibits for large values of N a periodic structure of narrow peaks, which are separated by 2π . While for odd values of N , all peaks are positive, for even values of N the peaks alternate between positive and negative values. The width of the peaks diminishes with increasing N . We may, thus, write the resulting phasematching function (where the phase term in Eq. 48 is to be neglected) for the crystal assembly as

$$\phi_N(\nu_s, \nu_i) = \phi(\nu_s, \nu_i) \chi(\nu_s, \nu_i; N) \quad (53)$$

where $\phi(\nu_s, \nu_i)$ represents the *single-crystal* phasematching function and $\chi(\nu_s, \nu_i; N)$ the crystal assembly contribution. If we express the phasemismatch as Taylor series considering only terms up to the first order, we obtain for the phase matching function the contributions

$$\chi(\nu_s, \nu_i; N) = \Upsilon_N \left(\frac{1}{2} [h\Delta \kappa^{(0)} + T_s \nu_s + T_i \nu_i] \right). \quad (54)$$

and

$$\phi(\nu_s, \nu_i) = \text{sinc} \left[\frac{L}{2} (\tau_s \nu_s + \tau_i \nu_i) \right] \quad (55)$$

where the τ_μ values are similar to T_μ [with $\mu = s, i$] (see Eq. 51), except for the absence of the spacer contribution:

$$\tau_\mu = [k'_p(2\omega_c) - k'_\mu(\omega_c)] L. \quad (56)$$

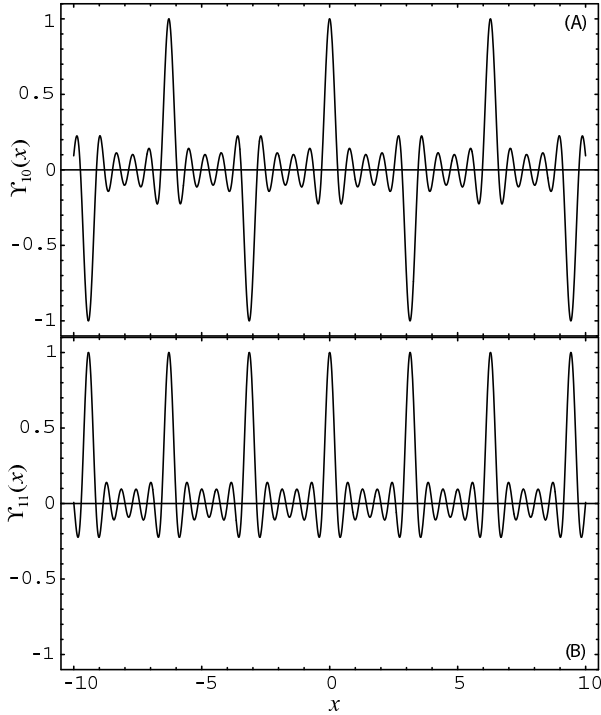


FIG. 4: Plots of the $\Upsilon_N(x)$ function showing different behavior for even and odd N ; while for even N , peaks alternate with valleys (separated by π) for odd N , there are no valleys. The peaks and valleys become narrower with increasing N . Such a function describes the phasematching contribution from the crystal-birefringent spacer sequence.

Let us now study the increased flexibility introduced into the two-photon state by such an assembly contribution to the phasematching function. We start our analysis by noting that the contours of the $\chi(\nu_s, \nu_i; N)$ function are straight lines oriented with a slope given by:

$$\tan \theta = -\frac{T_s}{T_i} = -\frac{(k'_p - k'_i)L + (\kappa'_p - \kappa'_i)h}{(k'_p - k'_s)L + (\kappa'_p - \kappa'_s)h} \quad (57)$$

Unlike for the case of a single crystal, where a change in crystal thickness merely results in an alteration of the spectral width (and further modifications to the phase-matching function cannot be attained except using different spectral regions or using different crystal materials), in the case of our crystal sequence source, the orientation of the spectral phasematching structure can be adjusted at will by varying the crystal to spacer thicknesses ratio L/h . The latter represents a very important added flexibility as it means that in principle an arbitrary orientation for the phasematching function orientation can be obtained.

To illustrate the power of such engineering of PDC we will discuss in the following the specific case of synthesizing a phasematching function with unit slope contours. As seen in section III A (see also [11]) such unit slope can result in spectrally decorrelated two-photon states. For the crystal assembly the inverse group velocities k'_μ, κ'_μ

(with $\mu = i, j$) evaluated at ω_0 and k'_p, κ'_p evaluated at $2\omega_0$, and the lengths L and h should satisfy the condition

$$(k'_s + k'_i - 2k'_p)L + (\kappa'_s + \kappa'_i - 2\kappa'_p)h = 0 \quad (58)$$

Eq. 58 closely resembles the group velocity matching condition [see Eq. 37]. In fact, this condition tells us that unit-slope phasematching contours require that a generalized group velocity condition be fulfilled: the weighted average (with crystal and spacer lengths as weighting factors) of the group velocity mismatch in the crystal and the spacer must vanish. Note that for this condition to be attainable, the spacer must exhibit a group velocity mismatch with the opposite sign as that of the crystal itself. A second condition which must be fulfilled relates to the constant phase term $h\Delta\kappa^{(0)}$ [see Eq. 50]. If such a term differs from a multiple of 2π , the maxima of the $\Upsilon_N(x)$ function can shift away from degeneracy (indeed by tuning such constant phase term, the resulting modes shift on the $\nu_s - \nu_i$ plane). Thus, a second condition on the spacer length which must be met is as follows:

$$h = \frac{2\pi m}{\Delta\kappa^{(0)}} \quad (59)$$

with m being an integer number. This tells us that the spacer length should be given as an integer multiple of the quantity $2\pi/\Delta\kappa^{(0)}$, which limits the minimum allowed spacer thickness. Thus, if the conditions expressed by Eqns. 58 and 59 are fulfilled, the crystal assembly phase-matching function can be written as:

$$\chi_N(\nu_s, \nu_i) = \Upsilon_N(T_-[\nu_s - \nu_i]) \quad (60)$$

where:

$$T_- = \frac{1}{2} ([k'_s(\omega_0) - k'_i(\omega_0)]L + [\kappa'_s(\omega_0) - \kappa'_i(\omega_0)]h). \quad (61)$$

Such a function consists of “ridges” (alternated with “trenches” for even N) described by unit-slope contours with a FWHM (along the $\nu_s - \nu_i$ direction) given, in the limit of large N , by

$$\delta\lambda = \frac{\sqrt{2}\lambda_0^2\gamma_2}{\pi cNT_-} \quad (62)$$

with $\gamma_2 = 1.39156..$ (this numerical value results from calculating the width of the $\Upsilon_n(x)$ function) and λ_0 denotes the central PDC wavelength. The maxima of different “ridges” result from the argument of the Υ_N yielding multiples of 2π . In the case studied here where group velocity matching is attained [see Eq. 58], the spectral separation between subsequent ridges along the $\nu - \nu_i$ direction can be shown to be given by

$$\Delta\lambda = \frac{\lambda_0^2}{\sqrt{2}cT_-}. \quad (63)$$

Note that the generation of spectrally decorrelated state actually necessitates a source with a single “ridge”; multiple ridges yields a joint spectral intensity with multiple

peaks in $\nu_s - \nu_i$ space which precludes spectral factorizability. Because a single ridge is not attainable with our crystal assembly source, we aim to let the separation between subsequent ridges be as large as possible so that the portion of the quantum state exhibiting the desired behavior can be isolated, e.g. by weak spectral filtering. We would like to emphasize that such spectral separation between subsequent ridges $\Delta\nu$ is inversely proportional to the parameter T_- , which in turn is proportional to the two thicknesses L and h . This leads to the manufacturing constraint that the individual crystal and spacer lengths should be as short as possible. As will be shown below this technique can indeed lead to a source of a decorrelated state with experimentally feasible crystal and spacer thicknesses.

Altogether the resulting joint spectral amplitude for the two-photon state produced by such a crystal assembly is therefore given by:

$$f(\nu_s, \nu_i) = \alpha(\nu_s + \nu_i)\phi(\nu_s, \nu_i)\chi(\nu_s, \nu_i; N) \quad (64)$$

where $\alpha(\nu_s + \nu_i)$ represents the pump envelope function, which is to be modelled as a Gaussian as in Eq. 20. Our approach is to let the bandwidth of the single crystal phasematching function $\phi(\nu_s, \nu_i)$ be much larger than that of the function $\chi(\omega_s, \omega_i; N)$, resulting from the crystal assembly. Thus, the spectral structure imposed on the phasematching function by the crystal assembly dominates over that of a single crystal. Given that the bandwidth of individual ridges of the function $\chi(\nu_s, \nu_i; n)$ depends inversely on N (while that of the function $\phi(\nu_s, \nu_i)$ does not depend on N), it is possible simply by using a large enough number of crystals to ensure that this condition on the widths of these two functions is fulfilled. Let us note that for the case of interest when the generalized group velocity matching condition [see Eq. 58] is satisfied, the orientations of $\chi(\nu_s, \nu_i; N)$ and that of the pump envelope function are orthogonal to each other (along the $\nu_s + \nu_i$ and $\nu_s - \nu_i$ directions respectively). This leads to the important conclusion that by choosing the pump bandwidth appropriately, a factorizable two-photon state can be obtained exhibiting nearly-circular contours. The value for the pump bandwidth σ which guarantees such factorizable behavior can be expressed, in terms of the number of crystal segments N and the parameter T_- (see Eq. 61) as:

$$\sigma = \frac{2\sqrt{2}}{\sqrt{\ln(2)}} \frac{\gamma_2}{NT_-}. \quad (65)$$

In summary, the proposed strategy for synthesizing a decorrelated two-photon state is as follows: i) The crystal and spacer materials should be chosen such that the group velocity mismatch for the crystal and spacer material have opposite signs. ii) The crystal and spacer thicknesses L and h should be chosen so that the generalized group velocity matching condition [see Eq. 58] is fulfilled and such that the constant phase term $\Delta\kappa^{(0)}$ vanishes [see Eq. 59]. Additionally, the crystal and spacer should

be thin enough so that the spectral separation between modes of the $\chi(\nu_s, \nu_i; N)$ function is large enough to ensure that a single resulting mode may be isolated. iii) The number of crystal segments N should be made large enough so that the phasematching bandwidth of a single crystal is much larger than that of the assembly phasematching function $\chi(\nu_s, \nu_i; N)$. iv) The pump should be prepared so that it exhibits a bandwidth σ which fulfils Eq. 65, thus guaranteeing that the pump envelope and phasematching functions are such that they yield a factorizable two-photon state.

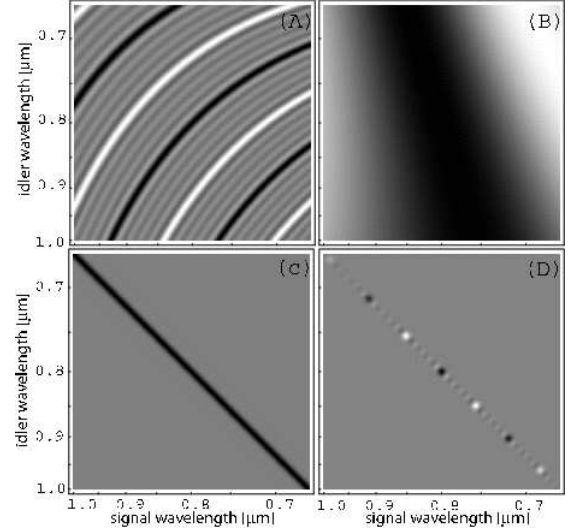


FIG. 5: (A) Assembly contribution to the phasematching function for the case of 10 BBO crystals with a cut angle of $\theta_c = 42.35^\circ$ (each with a thickness of $48.85\mu\text{m}$) alternated with 9 calcite spacers (each with a thickness of $58.83\mu\text{m}$). Black areas indicate positive values while white areas indicate negative values. (B) Phasematching function for single BBO crystal, with above characteristics. (C) Pump envelope function for pump field centered at 400nm with a bandwidth of 1.48nm . (D) Resulting joint spectral amplitude function.

We now study a specific example involving an assembly of BBO crystals and calcite spacers. Each of the crystals is characterized by a cut angle of $\theta_c = 42.35^\circ$ yielding type-II collinear degenerate phasematching at a central PDC wavelength of $\lambda_c = 800\text{nm}$. We remark that BBO and calcite exhibit the required opposite sign group velocity mismatch; for BBO: $2k'_p - k'_s - k'_i = 3.535 \times 10^{-4} \text{ps}/\mu\text{m}$ whereas for calcite: $2k'_p - k'_s - k'_i = -2.936 \times 10^{-4} \text{ps}/\mu\text{m}$. The generalized group velocity matching condition [see Eq. 58] tells us that the ratio of the calcite spacer thickness to the BBO crystal thickness should be $h/L = 1.204$. This yields a value for the minimum spacer thickness $2\pi/\Delta\kappa^{(0)} = 5.88\mu\text{m}$; we choose a value for the integer m [see Eq. 59] of 10, thus yielding a spacer thickness $h = 58.83\mu\text{m}$ and a BBO crystal thickness $L = 48.85\mu\text{m}$. These thicknesses yield a spacing between assembly phasematching modes (along the $\nu_s - \nu_i$ direction) of $\Delta\lambda = 67.05\text{nm}$, corresponding to a separation

along the ν_s or ν_i axes of 47.41nm. The latter means that over a bandwidth of 95nm around the central PDC wavelength (of 800nm) there is a single crystal-spacer assembly phasematching mode present. Fig. 5(A) shows a plot of the function $\chi(\nu_s, \nu_i; 10)$ for the above parameters, *i.e.* assuming that the assembly contains 10 BBO crystals and 9 calcite spacers. Note that near degeneracy (at $\lambda = 800\text{nm}$), the slope of the contours defining the function is indeed unity. Fig. 5(B) shows a plot of the phasematching function $\phi(\nu_s, \nu_i)$ for a single BBO crystal (with the above characteristics) making it clear that the spectral bandwidth exhibited is much larger than that of the assembly phasematching modes; the latter implies that the overall phasematching spectral structure is dominated by the assembly rather than the single crystal contribution. Fig. 5(C) shows the pump envelope function corresponding to a pump field with a center wavelength of 400nm and a spectral FWHM of 1.48nm, as required by Eq. 65 to yield a factorizable state. Fig. 5(D) shows the resulting joint spectral amplitude for our crystal assembly source. Due to the periodic character of the Υ_N function there are multiple modes, separated along each frequency axis by 47.4nm. Nevertheless, weak spectral filtering can isolate the central mode (centered at $\lambda_s = \lambda_i = 800\text{nm}$). Fig. 6 shows the joint spectral intensity corresponding to this central mode, clearly exhibiting spectral decorrelation.

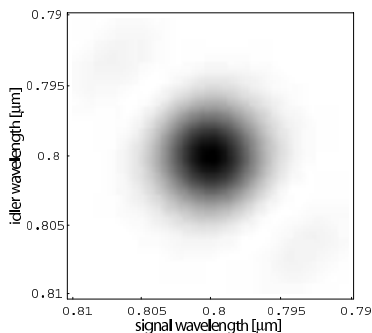


FIG. 6: This figure shows a the joint spectral intensity of the two-photon state produced by a sequence of 10 BBO crystals and 9 calcite spacers, as discussed in the text. The plot shows the region of the main degenerate peak near $\lambda_s = \lambda_i = 800\text{nm}$.

We have presented a novel technique which can yield factorizable states, based on group velocity matching compensation using a sequence of crystal segments alternated with bi-refringent spacers. The essential advantage of this approach is that it becomes in principle possible to synthesize a wide class of two-photon states simply by varying the spacer to crystal spacer thickness ratio, while choosing the crystal and spacer materials so that they obey certain relative dispersive properties. This scheme does not altogether eliminate the need for filtering; however, by reducing the crystal and spacer thicknesses L and h (and thus increasing $\Delta\lambda$; see Eq. 63) it becomes possible to increase the separation between modes, ideally to the point where in practice a single

mode is present. In the example shown above, the thicknesses were chosen in the region of $50\mu\text{m}$, since thinner segments may be difficult to manufacture and to handle. However, it is possible that by doping, ion exchange or some other process a single crystal may be modified in certain regions in such a manner that the group velocity mismatch changes sign; the modified regions would then play the role of the spacers, however in a single monolithic structure. With this approach it may be possible to take advantage of the smallest thicknesses allowed (with a value of $m = 1$ in Eq. 59), and thus eliminate the challenges likely to be faced in assembling a large number of thin crystals.

V. CONCLUSIONS

We have studied single photon conditional preparation based on photon pairs generated by the process of parametric downconversion. By modelling the detection as an appropriately defined projection operator we showed that, in general, the quantum state of the prepared state is described as a statistical mixture of the modes defined by the Schmidt decomposition of the PDC two-photon state. Furthermore, it was determined that a two photon state lacking correlations between the signal and idler photons, in all degrees of freedom, is a basic requirement for ideal single photon preparation, *i.e.* yielding quantum-mechanically pure single photons. Such pure single-photon wavepackets are of fundamental importance in experiments relying on quantum interference of single photons from distinct sources, as is the case in the recently proposed scheme for quantum computation with linear optics[4].

Assuming that spatial correlations can be independently eliminated (for example by the use of waveguided PDC[5]), we have discussed two techniques resulting in spectrally factorizable two-photon states. Firstly, it was shown that if an additional condition on the two photon state is fulfilled, the technique reported by Grice *et al.*[11] can yield a state in which both the joint *temporal* intensity, and the joint *spectral* intensity are factorable. The latter is crucial to guarantee full factorizability in two photon states designed for conditional preparation of single photons. Secondly, we have introduced a novel technique in which the group velocity mismatch between the pump and downconverted photons, responsible for the mixedness of the prepared single photons, can be controlled by using a sequence of crystals alternated with birefringent spacers exhibiting a dispersion which compensates that of the crystal in a specific manner. This represents a powerful technique in which spectrally decorrelated states, as well as a more general class of spectrally engineered two photon states, can be obtained simply by varying the relative thicknesses of the crystal and spacer used. These techniques described may provide useful tools for practical implementations of novel quantum-enhanced technologies, such as linear

optical quantum computation.

Acknowledgments

This work was funded in part by the EPSRC (CS, IAW), the US National Sciences Foundation ITR Pro-

gram (MGR, IAW, KB) the US Air Force Rome Laboratory (RE), the US Army Research Office through the MURI program (AU) and ARDA (WG, IAW). We gratefully acknowledge this support.

-
- [1] D. Bouwmeester *et al.*, 1997, Nature **390**, 575; D. Boschi *et al.*, 1998, Phys. Rev. Lett. **80**, 1121.
- [2] K. Mattle, H. Weinfurter, P.G. Kwiat and A. Zeilinger, 1996, Phys. Rev. Lett. **76**, 46564659.
- [3] See for example review: N. Gisin, G.G. Ribordy, W. Tittel and H. Zbinden, 2002, Rev. of Mod. Phys. **74**, 145
- [4] E. Knill, R. LaFlamme and G.J. Milburn, 2001, Nature **409**, 46; T.C. Ralph, A.G. White, W.J. Munro and G.J. Milburn, 2001, Phys. Rev. A **65**, 012314; T.B. Pittman, M.J. Fitch, B.C. Jacobs and J.D. Franson, 2003, quant-ph/0303095.
- [5] A.B. U'Ren, C. Silberhorn, K. Banaszek and I.A. Walmsley, 2004, Phys. Rev. Lett. **93**, 093601
- [6] U.M. Titulaer, R.J. Glauber, 1966, Phys. Rev. **145**, 1041.
- [7] Z. Bialynicka-Birula, 1968, Phys. Rev. **173**, 1207.
- [8] W.P. Grice and I.A. Walmsley, 1997, Phys. Rev. A, **56**, 1627.
- [9] C.K. Law, I.A. Walmsley and J. H. Eberly, 2000, Phys. Rev. Lett., **84**, 5304.
- [10] H. Huang and J.H. Eberly, 1993, J. Mod. Opt., **40**, 915
- [11] W.P. Grice, A.B. U'Ren and I.A. Walmsley, 2001, Phys. Rev. A **64**, 063815
- [12] T.E. Keller and M.H. Rubin, 1997, Phys. Rev. A, **56**, 1534
- [13] C.K. Hong, Z.Y. Ou and L. Mandel, 1987, Phys. Rev. Lett., **59**, 2044
- [14] A.B. U'Ren, K. Banaszek and I.A. Walmsley, 2003, Quantum Information and Computation **3**, 480.
- [15] Z.D. Walton, A.V. Sergienko, B.E.A. Saleh and M.C. Teich, 2004, Phys. Rev. A **70**, 052317
- [16] V. Giovannetti and L. Maccone and J. H. Shapiro and F. N. C. Wong, 2002, Phys. Rev. A, **66**, 043813.
- [17] J. Rarity and T. Wall and K. Ridley and P. Owens and P. Tapster, 2000, Appl. Opt., **39**, 6746.
- [18] A.B. U'Ren, C. Silberhorn, K. Banaszek, I.A. Walmsley, to be published.
- [19] Periodically poling of the $\chi^{(2)}$ -nonlinearity essentially allows to achieve quasi-phasematching at arbitrary wavelengths
- [20] In case of a degenerate type-I process $\beta_s = \beta_i$
- [21] Assuming the spectral bandwidth of the pump is large enough that the phase-matching function dominates over the pump envelope function